13th World Conference on Earthquake Engineering
Vancouver, B.C., Canada
August 1-6, 2004
Paper No. 1885

CHARACTERISTICS OF PIEZOELECTRIC DAMPERS AND THEIR APPLICATION TO TALL BUILDINGS AS A SMART STRUCTURAL SYSTEM

Yoshikazu KITAGAWA [1], Hiroyuki TAMAI [2] and Masaki TAKESHITA[3]

SUMMARY

Piezoelectric materials can be applied not only to sensors and actuators in a smart structural system, but also to dampers. A previous study proposed a conceptual design for a smart structural system that uses smart materials, and described how the innate performance of piezoelectric materials, called smart materials, can be used to make actuators, sensors, and dampers [1]. In this current study, first, vibration tests were used to evaluate the performance of a scaled cantilever beam and portal frame containing piezoelectric materials, and then the performance of piezoelectric dampers as part of a smart structural system for buildings was evaluated.

INTRODUCTION

Artificial life has recently been extensively researched, focusing on evolution, shape formation, learning, distributed parallel biological processing, immunity, and self-remodeling [2,3]. As one of the basic mathematical functions of artificial life, genetic algorithms based on the principle of biological evolution (i.e., selection, crossover, and mutation) are used to model the evolution process. Among these possible processing functions, evolution is the most useful method for optimization, because smart structural systems respond according to simple internal principles and through interactions with outside sensors, and not by external instructions. Thus, self-organization of system is independent from the system order. Also, self-formation is the mapping from a genetic type to an expressing type, and has the important role of enhancing the robustness of the system adaptability.

In designing and controlling large-sized, complicated response-control systems for buildings that are in uncertain and changing environments, it is impossible to provide control algorithms and data that can handle every control scenario. As the complexity of the control system increases, the possibility of providing accurate and comprehensive information decreases, thus degrading the responsiveness, reliability, safety, and robustness of the system. To avoid such degradation in accuracy and comprehensiveness, the development of smart structural systems that use these control systems is needed.

[1] Professor, Faculty of Science and Technology, Keio University, Dr. of Eng.,
Email: kitagawa@sd.keio.ac.jp
[2] Associate Professor, Faculty of Engineering, Hiroshima Institute of Technology, Dr. of Eng.
[3] Research Engineer, Ando Corporation, Dr. of Eng.

Currently, earthquake disaster countermeasures for buildings are seismic design and response control devices, such as actuators and sensors. Monitoring is also a must for maintaining and controlling such response control devices. In the future, incorporation of genetic algorithms into response control systems will make the self-organization of systems and their organic optimization economically possible.
Consequently, introducing smart structural systems into buildings is practicable only when coupled with the development of smart materials. Structural interpretation for the aspects of artificial life (e.g., evolution, shape, formation, learning) will coincide with the development of technology related to each aspect. Incorporating smart structural systems into buildings is the future of earthquake countermeasures.
To develop a comprehensive smart structural system, it is necessary to focus on either the innate characteristics of the material itself or on a combination of computational and mechanical technology that combines sensors, actuators, data processing, and expression. Controllable materials considered promising for optimum applications in controlling large-sized and complicated building structures used in smart structural systems are piezoelectric, magnet-strictive, magnet-rheological-fluid (MRF), electro-rheological-fluid (ERF), and shape-memory alloys (SMA) materials, which have been used in aeronautical engineering.
In this study, the characteristics of piezoelectric dampers built with piezoelectric materials are investigated as part of a smart structural system for buildings. Here, first the damping mechanism and complex stiffness of a piezoelectric damper were derived from the piezoelectric equations. Then, an equation used to evaluate the damping performance for building structures with piezoelectric dampers was derived. To demonstrate how the innate performance of piezoelectric materials, called smart material, can be utilized in a smart structural system, the vibration tests were used to evaluate the performance of a scaled cantilever beam and portal frame. Finally, to determine the applicability and availability of piezoelectric dampers, the habitability of an actual high-rise steel apartment building with piezoelectric dampers to strong wind was evaluated.

PIEZOELECTRIC DAMPER AND ITS DAMPING-EVALUATION EQUATIONS

Mechanism of piezoelectric damper

Figure 1 shows a schematic of a piezoelectric damper. The piezoelectric material converts mechanical energy into electric energy when the material is strained. This phenomenon is called the piezoelectric effect. A piezoelectric material can be applied as a strain sensor to detect the electric current or voltage caused by the piezoelectric effect. By shunting an appropriate circuit to the piezoelectric material, electric energy caused by the mechanical energy will be consumed as heat energy. As a result, mechanical energy inputted into a building structure in which piezoelectric dampers are installed is dissipated, resulting in a damping effect. The piezoelectric damper considered here consists of piezoelectric material and a shunted circuit (resistor, inductor and capacitor).

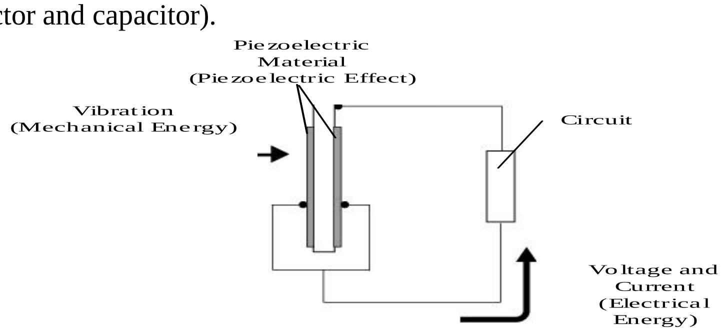

Figure 1: Schematic of a piezoelectric damper

The mechanism of a piezoelectric damper can simply be described by use of complex stiffness. In general, a piezoelectric material with complex stiffness can be evaluated by using the energy consumption ratio and damping factor from a phase angle diagram corresponding to its real and imaginary parts. The phase angle varies depending on frequency, electrical impedance of the shunted circuit, and the properties of the piezoelectric material. Thus, the damping factor and effective stiffness of the damper are controllable by adjusting the frequency and electrical impedance.

Damping evaluation expression for a structure containing a damper

Figure 2 shows the shunted circuit in a piezoelectric damper with impedance ^{ADD}Z. This impedance is treated as a piezoelectric material with overall impedance $^{RE}\mathbf{Z}$ (3x3 components). Assuming no external electrical input, the complex stiffness matrix of piezoelectric damper, $^{RE}\mathbf{Y}$, is obtained as follows [4].

$$^{RE}\mathbf{Y} = \left[{}_{E}\mathbf{s} - \tilde{i}\,\omega \cdot \mathbf{d}^{\mathbf{T}} \cdot \ell^{-1} \cdot {}^{RE}\mathbf{Z} \cdot \mathbf{A} \cdot \mathbf{d} \right]^{-1} \tag{1}$$

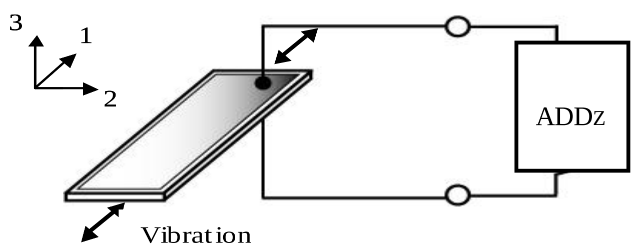

Figure 2: Piezoelectric material connected with a shunted circuit

where ${}_{E}\mathbf{s}$ is the compliance matrix for the piezoelectric material where the electrical field, *E*, is constant (6x6 components), $\tilde{i}$ is imaginary unit, ω is circular frequency, ℓ is the diagonal matrix for electrode length (3x3 components), **d** is the matrix for piezoelectric material constants (3x6 components), **A** is the matrix of the surface areas of piezoelectric material, and $(\ )^{T}$ denotes transpose of a matrix.

For a circuit consisting of a resistor and an inductor shunted in the polling direction of the piezoelectric material (direction 3) as shown in Fig. 3, the relevant component of overall impedance, $^{RE}Z_{33}$, is given as follows.

$$^{RE}Z_{33} = \frac{1}{a_Z{}^2 + b_Z{}^2} \cdot \left(a_Z - \tilde{i} \cdot b_Z \right) \tag{2}$$

where

$$a_Z = \frac{R}{R^2 + \omega^2 \cdot L^2} \tag{3.a}$$

$$b_Z = \omega \cdot {}_{T}C_{P,3} - \frac{\omega \cdot L}{R^2 + \omega^2 \cdot L^2} \tag{3.b}$$

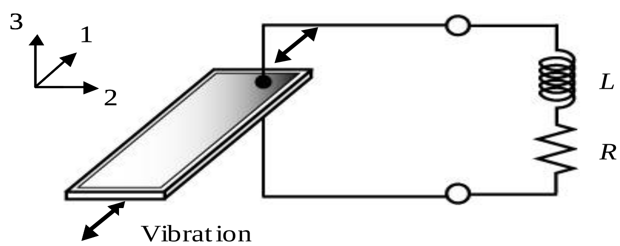

Figure 3: Piezoelectric material connected with inductor, *L*, and resistor, *R*.

where R and L denote resistance and inductance of the circuit, respectively, and ${}_{T}C_{P,3}$ denotes capacitance of the piezoelectric material, where stress, T, is constant, in direction 3.

Noting that the strained direction is direction 1, the relevant stiffness component of a piezoelectric damper, ${}^{RE}Y_{11}$, is derived from Eqs. (1),(2), and (3.a,b) as follows.

$$ {}^{RE}Y_{11} = {}_{E}Y_{11} \cdot \frac{1}{a_{LR}{}^{2} + b_{LR}{}^{2}} \cdot \left(a_{LR} + \tilde{i} \cdot b_{LR} \right) \tag{4} $$

where

$$ a_{LR} = 1 - \frac{\omega \cdot {}_{T}C_{P,3} \cdot k_{31}{}^{2} \cdot d_{LR}}{c_{LR}{}^{2} + d_{LR}{}^{2}} \tag{5.a} $$

$$ b_{LR} = \frac{\omega \cdot {}_{T}C_{P,3} \cdot k_{31}{}^{2} \cdot c_{LR}}{c_{LR}{}^{2} + d_{LR}{}^{2}} \tag{5.b} $$

$$ c_{LR} = \frac{R}{R^{2} + \omega^{2} \cdot L^{2}} \tag{5.c} $$

$$ d_{LR} = \omega \cdot {}_{T}C_{P,3} - \frac{\omega \cdot L}{R^{2} + \omega^{2} \cdot L^{2}} \tag{5.d} $$

where k_{31} and ${}_{E}Y_{11}$ are electromechanical coupling coefficient and Young's modulus, respectively, for a piezoelectric material where E is constant.

Damping factor of the damper, β, is simply given from the phase angle for the imaginary and real parts of ${}^{RE}Y_{11}$ as follows.

$$ \beta = \sin\left(\frac{1}{2} \cdot \tan^{-1} \frac{\mathbf{Im}\left({}^{RE}Y_{11}\right)}{\mathbf{Re}\left({}^{RE}Y_{11}\right)} \right) \tag{6} $$

Eqs.(4) and (6) suggest that relatively large damping by the damper can be achieved in the low frequency range by adjusting the resistance, R, and inductance, L.

Because damping factor, β, represents the damping performance for a fundamental vibration system, it is impossible to evaluate the damping performance for a building structure that contains piezoelectric dampers by only using Eqs.(4) and (6). Therefore, we introduce Biggs's formula to evaluate the damping factor for the total system.

For n dampers attached to a building structure, Biggs's formula yields the following relation between damping ratio and energy dissipation ratio for the i-th piezoelectric damper and total system.

$$ \beta_{i} = \frac{1}{4\pi} \cdot \frac{\Delta W_{P,i}}{W_{P,i}} \quad , \quad \Delta h = \frac{1}{4\pi} \cdot \frac{\sum_{i=1}^{n} \Delta W_{P,i}}{W} \tag{7.a,b} $$

where β_{i} , $\Delta W_{P,i}$, $W_{P,i}$ are damping factor, energy dissipation per cycle, and maximum strain energy for the i-th damper, and Δh , W are damping factor and maximum strain energy for the total system.

Substituting Eq.(7.a) into Eq.(7.b) yields the additional damping factor due to the damper for the total system, Δh:

$$ \Delta h = \frac{\sum_{i=1}^{n} \beta_{i} \cdot W_{P,i}}{W} \tag{8} $$

Because this equation involves only the energy dissipation ratio $\Delta W_{P,i} / W_{P,I}$ and damping factor β_i of the damper, it is easily applied to situations where modulation of natural frequency and variation of natural modes occur.

VIBRATION TESTS

Outline of Tests

To demonstrate the applicability of piezoelectric materials for sensing, actuating and damping, three types of vibration tests were carried out.

In the vibration tests to verify the sensing and actuating functions, a bimorph (Fig.4) consisting of a steel plate and two piezoelectric plates was installed in the fixed end of a cantilevered beam (Fig.5). Figure 6 shows the actuating systems, as an example, used to evaluate the sensing and actuating functions of piezoelectric materials.

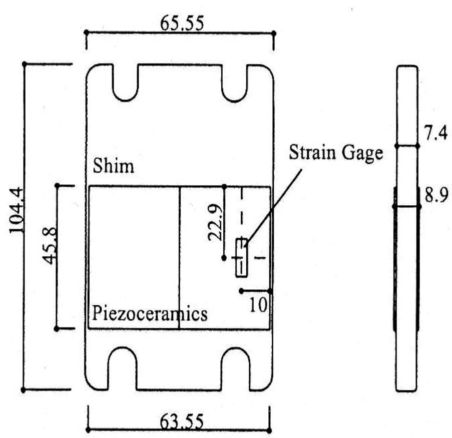

Figure 4: Detail of bimorph

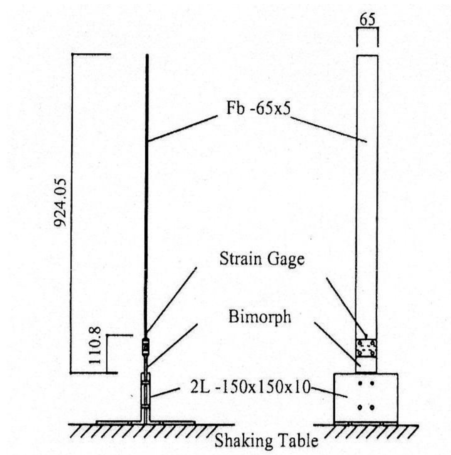

Figure 5: Cantilevered beam specimen (Type A specimen)

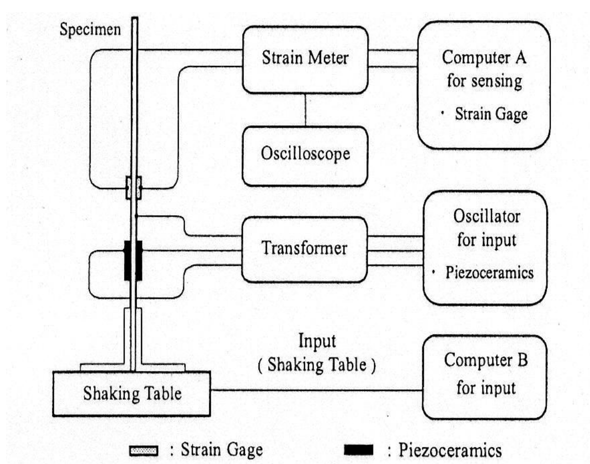

Figure 6: System for evaluating both the sensing function and actuating function of piezoelectric material

The material and electrical properties of the piezoceramic are shown in Table 1.

Table 1: Mechanical and electrical properties of piezoceramic used in bimorph

Lead Zircotitanete Ceramics ($PbZrO_3$-$PbTiO_3$)		
Young's Modulus	E_{11}	5.8×10^{10} (N/m^2)
Poisson's Ratio	ν	0.35
Relative Dielectric Constant $\chi_o = 8.854 \times 10^{-12}$ (F/m)	χ_{33}/χ_o	2000
Piezoelectric Constant	d_{31}	195×10^{-12}(m/V)
Electro-mechanical Coupling Cofficient	k_{31}	0.35
Static Capacitance (Bimorph has 4 Piezocramics)	C	120(nF) , (=4x30nF)

In the damping verification tests, the portal frame and system shown in Figs.7 and 8, were used.

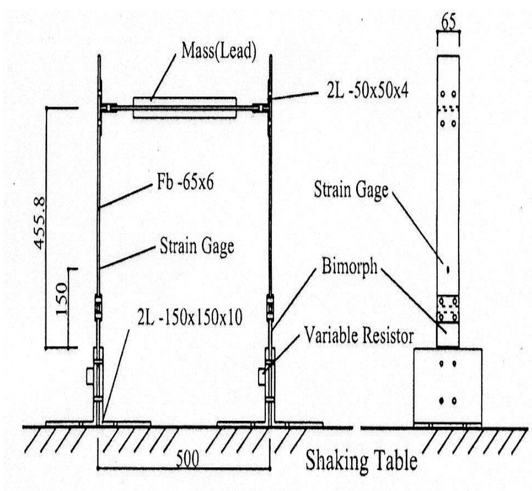

Figure 7: Portal frame specimen (Type B specimen)

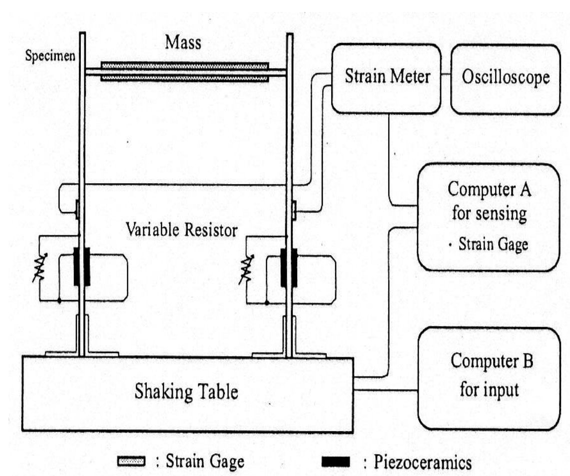

Figure 8: System for evaluating damping function

A bimorph similar to that installed in the beam was installed in the end of the portal frame columns. For the bimorphs installed in the portal frame columns, however, an adjustable resistor was used to shunt the piezoceramic electrodes. In all tests, the strain, ε , was measured at the fixed end, and the excitation was done using a shaking table. In the actuating and damping verification tests, excitation was four sinusoidal cycles at the system's natural frequencies, *f*, of 6.0 Hz and 12.8Hz. In actuating verification tests, an AC voltage of 250V and an inverse phase of 6.09Hz were applied to the piezoelectric materials.
The damping ratio, h, in each test was calculated from vibration data measured for free vibrations, by using a least-square method based on the following equation:

$$\left|\varepsilon_a(t)\right| = a \cdot \exp\left\{ -\mathrm{h} \cdot \frac{2\pi}{\mathrm{T}_1} \cdot t \right\} \tag{9}$$

where $\left|\varepsilon_a\right|$ is the strain amplitude, t is time, a is the amplitude at t = 0 and T_1 is the natural period.

Under steady-state vibrations, the equivalent damping ratio added by the piezoelectric damper without an inductor in the circuit, h_{add}, is obtained as follows [4,5].

$$h_{add} = \frac{\eta}{2} \cdot \frac{\upsilon_\rho}{\upsilon} \tag{10}$$

where,

$$\eta\ (f) = \frac{\rho \cdot k_{31}^2}{(1 - k_{31}^2) + \rho^2} \tag{11a}$$

$$\rho = \mathrm{R} \cdot \mathrm{C}\left(1 - k_{31}^2\right) \cdot 2\pi \cdot f \tag{11b}$$

where υ_ρ and υ denote peak strain energy in the piezoelectric material and total system, respectively, η is loss factor , ρ is non-dimensional frequency, R is resistance, C is static capacity, and f is frequency of excitation.

The optimum resistance, R_{Out}, that maximizes h_{add} can be determined as follows.

$$\frac{\partial h_{add}}{\partial R} = 0 \tag{12}$$

Consequently,

$$\mathrm{R}_{opt}(f) = \frac{1}{\mathrm{C}\sqrt{(1 - k_{31}^2)} \cdot 2\pi \cdot f} \tag{13}$$

Test Results

Figures 9 (a) and (b) show results for actuating tests for the temporal vibration of strain near the fixed end with and without actuation, respectively. In Fig. 9, $\varepsilon/\varepsilon_a^*$ represents ε normalized by the strain measured when the maximum displacement of the specimen reaches 1.0 cm, and t/T_1 represents t normalized by the natural period T_1. Figures 10 (a) and (b) show the results from the damping tests as R/R_{out} vs. h, in which R_{out} was calculated from Eq. (13) and h was calculated from Eq. (9), and show the results for R/R_{out} and $h_{add} + h_{inh}$ calculated from Eq. (10). The results shown in Fig. 10(a) correspond to R/R_{out} from 0 to 10 and those in Fig. 10(b) correspond to R/R_{out} from 0 to 2.

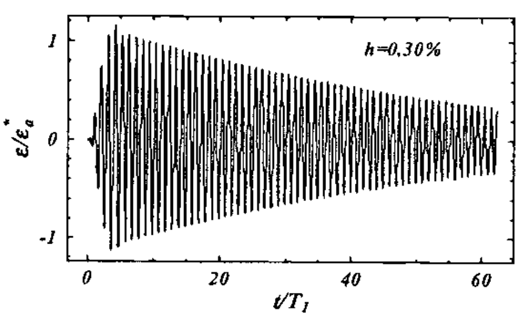

Figure 9(a): Strain with piezoelectric actuator

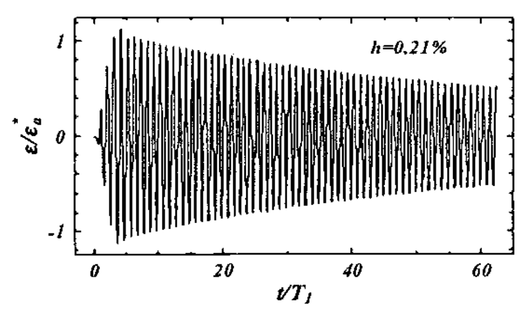

Figure 9(b): Strain without piezoelectric actuator

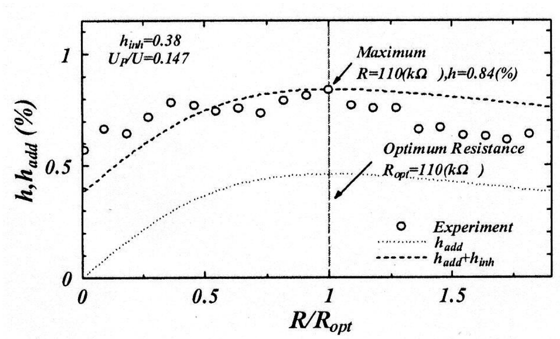

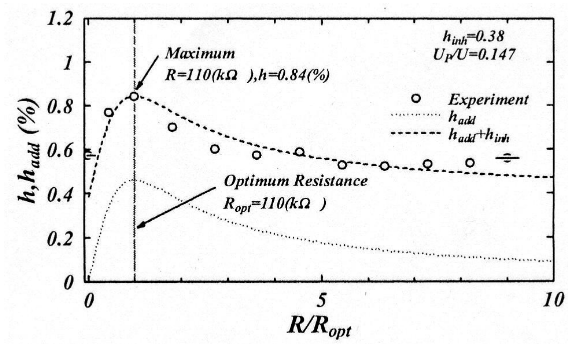

(a): f =6.0Hz (b): f =11.0Hz

Figure 10(a) (b): Damping $h_{,add}$ *and h vs*. resistance ratio R/R_{out}

Based on these results, the optimum resistance of the piezoelectric damper that maximized the damping ratio was accurately predicted by Eq. (13), and when the damping was attached to over only 10% of the column area, the piezoelectric damper increased the damping ratio by 30% compared with its in inherent damping ratio.

DAMPING PERFORMANCE OF A TEST BUILDING

Test building

The test building was the high-rise steel apartment [6] and can be summarized as follows.

Main structure: Steel structure (all columns are concrete-filled steel tubes)
Floors: 30 upper floors, 1 basement floor
Natural frequency: 0.353 Hz
Height: 94.5 m
Weight per floor: 1200kg/m^2

Table 2 shows cross-sectional properties of a column and beam in this building. Figure 11 shows the structural and beam plan of the building. The properties of the columns (concrete-filled steel tubes) are normalized by Young's modulus for steel.

Table 2: Column and beam sectional properties[5]

Column (Concrete filling square tube)			
	floor	sectional area	moment of inertia
mm		m^2	m^4
□ -850x32	1-15	0.22826	0.01806
□ -850x25	16-22	0.21050	0.01619
□ -850x22	23-30	0.20279	0.01537

Beam			
	floor	sectional area	moment of inertia
mm		m^2	m^4
H-800x350x22x32	1-15	0.03859	0.00404
H-1000x350x19x32	16	0.04018	0.00655
H-750x350x19x32	17-23	0.03070	0.00300
H-700x350x14x25	24-31	0.02660	0.00231

Wind velocity as external disturbance

The 10-minute average wind velocity of the annual recurrence interval at the top of the building, V_T, is given as follows [7, 8].

$$V_T = \frac{E(H_A)}{E(H_T)} \cdot V_A \tag{14}$$

where H_A is the height of the observation point, V_A is the 10-minute average wind velocity of the annual recurrence interval at the observation point, and $E(H_A)$ and $E(H_T)$ are vertical wind profiles at the observation point and building location, respectively.

V_A and H_A at the Hiroshima Local Meteorological Observatory are 13.9m/s and 19.5m, respectively. For $E(H_A)$ = 0.69 and $E(H_T)$ = 1.40, then from Eq.(14), V_T = 28.1m/s.

Evaluation method of maximum response acceleration

For a high-rise rectangular-plan building, the cross-wind response is much greater than the with-the-wind response. Therefore, we consider only the cross-wind response. The maximum acceleration for the cross-wind direction at the top of the rectangular-plan building, A_{max} , is given as follows [9].

$$A_{\max} = \frac{2 \cdot C_A \cdot g_A}{3} \cdot \left(\frac{V_T}{f_1 \cdot \sqrt{B \cdot D}} \right)^{3.3} \cdot f_1^2 \cdot \sqrt{B \cdot D} \cdot \frac{\rho_A}{\rho \cdot \sqrt{h}} \tag{10.a}$$

$$g_A = \sqrt{2 \cdot \log(f_1 \cdot T_W)} + \frac{0.577}{\sqrt{2 \cdot \log(f_1 \cdot T_W)}} \tag{10.b}$$

where B and D are the width and depth of the building, ρ_A is the air density (1.23kgf/m^3), h and ρ are damping factor and average density of the building, C_A is a constant of 0.6, g_A is the peak factor, f_1 is the natural frequency, and T_w is the evaluation time (600 seconds).

Substituting h=0.01, f_1=0.353Hz, B=34.0m, and D=34.0m into Eq.(10.a) yields A_{max} = 36.8mm/s^2 for the test building with no dampers[5]

Layout of dampers and damper parameters

The piezoelectric dampers installed in the test building were composed of piezoelectric material, a resistor, and an inductor. In our evaluation, the cross-wind response to a strong wind in direction 2 was considered as shown in Fig. 11. Therefore, the piezoelectric dampers were installed in beams and columns along the direction-1 structural plane, as shown in Fig.12. The piezoelectric materials were also installed in the outside flanges of the columns and the inside flanges of the beams.

The layout and shape of piezoelectric materials in the tests were defined as follows. The thickness of the piezoelectric material, t_P, was determined by a fixed ratio with respect to the flange thickness of the steel member, t_P/t_S. The length of the piezoelectric material, ℓ_P, was determined by a fixed ratio with respect to the length of the steel beam and column, ℓ_P/ℓ_S. The width of the piezoelectric material in the column, b_{CP}, was equal to the width of the steel column, b_S, and the width, b_{BP} , was equal to the width of the flange minus the thickness of the web. The real part of stiffness for the piezoelectric material, $\boldsymbol{Re}({}^{RE}Y_{11})$, was determined by the ratio with respect to Young's modulus for steel, α (=$\boldsymbol{Re}({}^{RE}Y_{11})/Y_S$, Y_S=206GPa). For simplicity, the capacitance, electro-mechanical coupling coefficient of piezoelectric material, resistance, and inductance were specified in accordance with β_i. Consequently, the additional damping factor due to the damper, Δh, was calculated from these parameters.

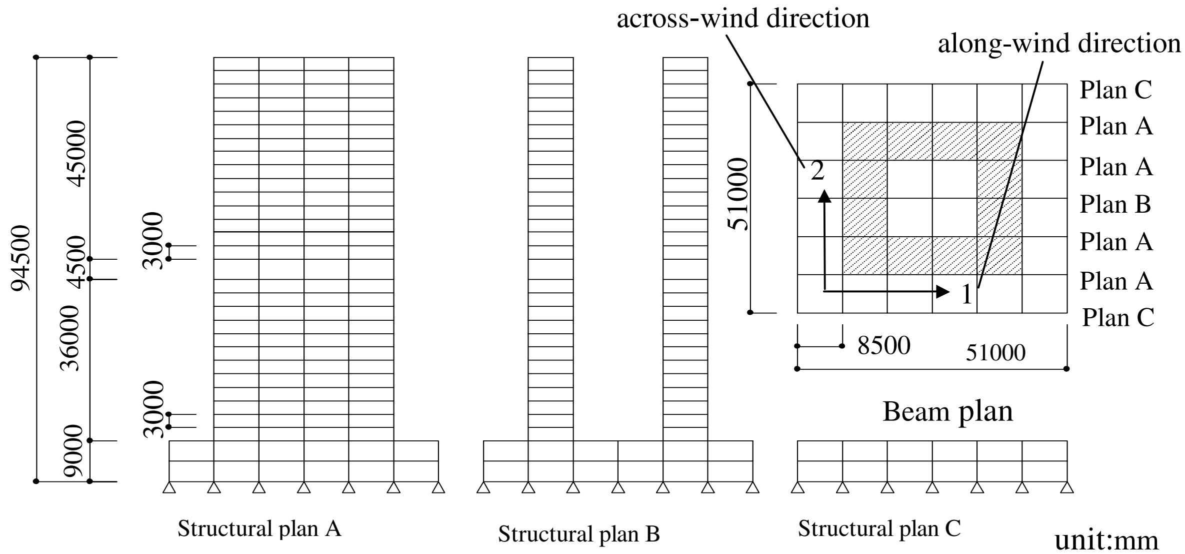

Figure 11: Structural plan and beam plan of test building structure[5]

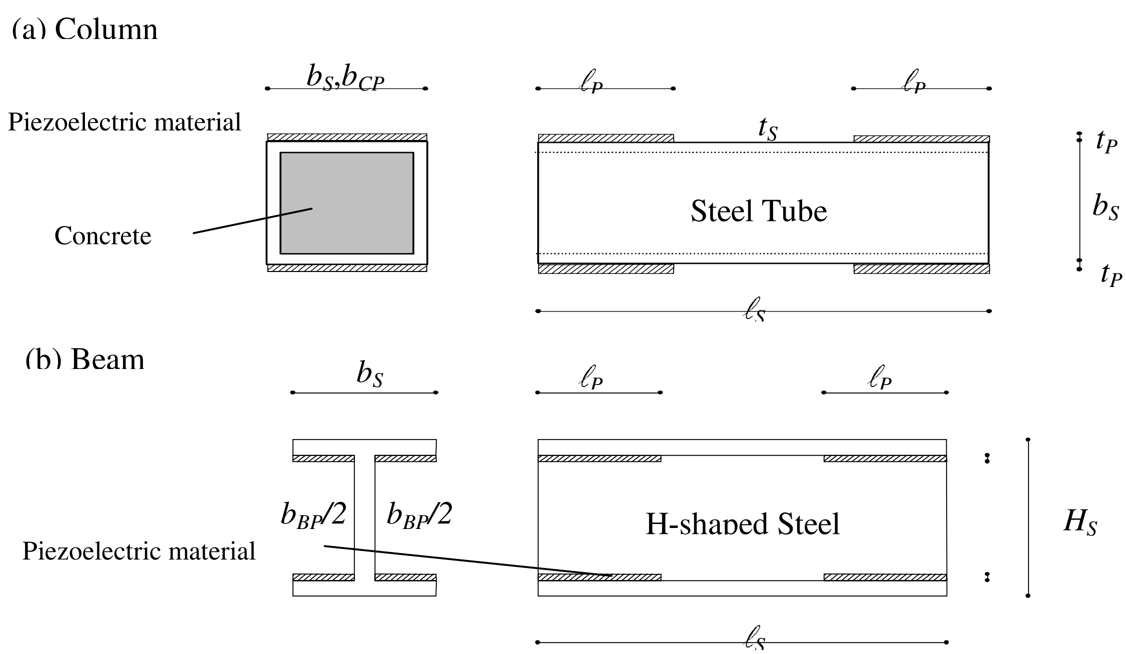

Figure 12: Layout of piezoelectric material

Series of tests

Three series of damper parameters were tested in the building. Table 3 lists the parameters for each series A, B, and C. In all three series, $\alpha = 0.15$, $\beta = 0.6$, and ℓ_P/ℓ_S ranged from 0.1 to 0.5. In series A, B, and C,

t_p/t_s = 0.1, 0.5, and 0.1, respectively. Because the piezoelectric material was installed at both ends of a member, ℓ_p/ℓ_S =0.5 means that the piezoelectric material was installed in all flanges.

Table 3: Parameters of series A, B, C

	$\alpha = \boldsymbol{Re}(^{RE}Y_{11})/Y_S$	β	t_P/t_S	ℓ_P/ℓ_S
series A	0.15	0.6	0.1	0.1~0.5
series B	0.15	0.6	0.5	0.1~0.5
series C	0.15	0.6	1	0.1~0.5

The maximum acceleration for the cross-wind direction, A_{max}, was obtained by the following four steps. (1) Eigenvalue analysis of the building was done, and then the natural frequency and first natural mode were calculated. In the eigenvalue analysis, the modulus of longitudinal elasticity for piezoelectric material was $\boldsymbol{ABS}(^{RE}Y_{11})$. (2) The building was strained with first natural mode deformation, and then the ratio between the maximum strain energy of the piezoelectric material, W_P , and the maximum strain energy of total system, W, was calculated. In the static analysis, modulus of longitudinal elasticity for the piezoelectric material was $\boldsymbol{Re}(^{RE}Y_{11})$. (3) The additional damping factor, Δh, was obtained by substituting (W_p/W) and β into Eq.(8). (4) Natural frequency, f_1, and damping factor that included the inherent damping factor (0.01), for the total system (0.01+Δh) were substituted into Eq.(15), thus yielding the value for A_{max}. Figure 13 shows f_1 vs. A_{max} for series A, as an example, with and without piezoelectric dampers. The lines H-1, H-2, H-3, and H-4 denote grades of building habitability set in guidelines by AIJ[7]. For habitability, A_{max} that falls below the H-2 lines is desired for high-rise apartment buildings. Figure 14 shows ℓ_p/ℓ_S vs. Δh for all three series.

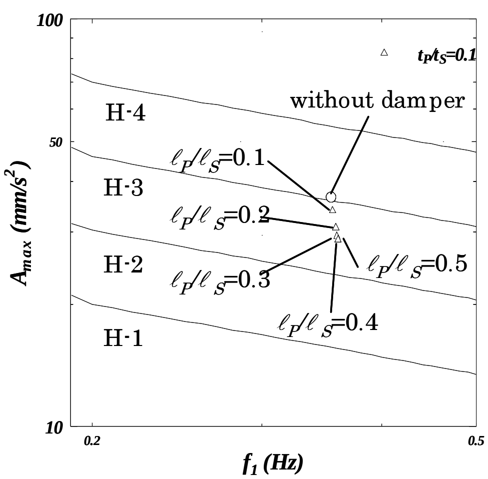

Figure 13: Maximum acceleration A_{max} (series A) vs. natural frequency f_1

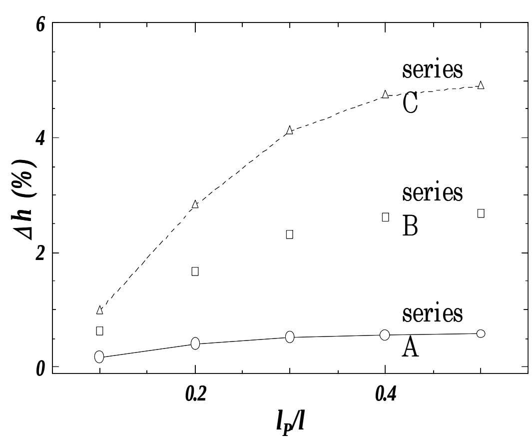

Figure 14: Additional damping factor Δh vs. ℓ_P/ℓ_S

The results can be summarized as follows.

i) When t_p/t_S > 0.5 and ℓ_p/ℓ_S > 0.2, A_{max} was below the H-2 line. When t_p/t_S=0.5 and ℓ_p/ℓ_S =0.2, A_{max} half that without dampers.

ii) Natural frequency, f_1, increased with increasing ℓ_p/ℓ_S and t_p/t_S .

iii） Additional damping factor, Δh, increased with increasing ℓ_p/ℓ_S and t_p/t_S.

iv） A higher t_p/t_S yielded higher Δh and lower A_{max}. However, increasing ℓ_p/ℓ_S to above 0.4 yielded no further improvement in either Δh or A_{max}.

v） Habitability of the building frame was improved economically and effectively by installing piezoelectric material along 30% of the length from the end of the beams and columns.

vi） Piezoelectric dampers enabled the test high-rise apartment building of practical dimensions to satisfy the H-2 grade habitability.

CONCLUSIONS

Piezoelectric dampers built with piezoelectric materials were characterized as part of a smart structural system for buildings. First, the damping mechanism and complex stiffness for a piezoelectric damper were derived from piezoelectric equations. Then, to demonstrate how piezoelectric materials can be incorporated into smart material systems, vibration tests were used to evaluate the performance of a scaled cantilevered beam and a portal frame. The vibration test results validated the control systems and demonstrated how to determine the characteristics and performance of piezoelectric materials for use in dampers in smart material systems. Finally, to determine the applicability and availability of piezoelectric dampers, the habitability of an actual high-rise steel apartment building incorporated with piezoelectric dampers exposed to strong wind was evaluated.

In conclusion, the performance of smart structural systems depends on the smart materials, which have been developed mainly from a practical-use viewpoint. When a consensus on the requirement of future smart structure systems is reached, incorporation of smart materials into future smart systems will proceed. Development of reliable smart material technology and methods for evaluating the vulnerability of each component of smart structural systems is therefore crucial.

ACKNOWLEDGMENTS

This work was supported by a Grant-in-Aid from the Ministry of Education, Science and Culture of Japan (No.09490027 and 13450227)

REFERENCES

1. Kitagawa.Y,Tamai.H and Takeshita.M, Smart structural systems for exposed to external disturbances － Concept and Technology ,12WCEE(2000)
2. C.Labgton , Artificial life, Santa Fe (1989)
3. K.Kitano , Artificial life and combination of evolution, generation and learning, Mathematic Science vol.353 (1992)
4. N.W.Hagood and A.V.Flowtow, Damping of structural vibrations with piezoelectric materials and passive networks, Journal of SV vol.146, No.2 pp.243-268 (1991)
5. N.W.Hagood and E.F.Crawley, Approximate frequency domain analysis for damped space structures, Journal of AIAA vol.28, pp.1963-1961 (1990)
6. Report of study on steel high-rise apartment (in Japanese), Chugoku branch of AIJ (1996)
7. Guidelines for the evolution of habitability to building vibration (in Japanese), AIJ (1991)
8. Recommendation for loads on building, AIJ (1991)
9. Report on evaluation of habitability for high-rise apartment under strong (in Japanese), HUDC (1991)